

## BIOPHYSICS

# Flies trade off stability and performance via adaptive compensation to wing damage

Wael Salem<sup>1</sup>, Benjamin Cellini<sup>1</sup>, Heiko Kabutz<sup>2</sup>, Hari Krishna Hari Prasad<sup>2</sup>, Bo Cheng<sup>1</sup>, Kaushik Jayaram<sup>2</sup>, Jean-Michel Mongeau<sup>1\*</sup>

Physical injury often impairs mobility, which can have dire consequences for survival in animals. Revealing mechanisms of robust biological intelligence to prevent system failure can provide critical insights into how complex brains generate adaptive movement and inspiration to design fault-tolerant robots. For flying animals, physical injury to a wing can have severe consequences, as flight is inherently unstable. Using a virtual reality flight arena, we studied how flying fruit flies compensate for damage to one wing. By combining experimental and mathematical methods, we show that flies compensate for wing damage by corrective wing movement modulated by closed-loop sensing and robust mechanics. Injured flies actively increase damping and, in doing so, modestly decrease flight performance but fly as stably as uninjured flies. Quantifying responses to injury can uncover the flexibility and robustness of biological systems while informing the development of bio-inspired fault-tolerant strategies.

## INTRODUCTION

A hallmark of biological systems is their ability to compensate for perturbations, whether of internal or external origins. Environmental perturbations can have severe consequences for survival, in some instances causing injury that impairs mobility (1). In arthropods, damage can arise from molting defects, disease, predation, aggression for mate selection, etc. A survey of arthropod natural populations revealed that 40% of certain arthropod species are missing at least one whole appendage (2); therefore, perturbations can be the norm rather than the exception. For flying insects, internal perturbations such as wing damage can have dire consequences that affect overall flight performance (1, 3, 4). When a single wing is damaged, the situation could be catastrophic, as asymmetric aerodynamic forces could rapidly destabilize the body.

The response of flying insects to wing damage can provide critical insights into flight-control mechanisms as changes in aerodynamic surface translate to changes in forces and moments of the center of mass. Wing damage can arise from wear or predation and directly influences mortality (1, 5, 6); thus, flying insects have likely evolved a host of compensatory mechanisms to maintain fitness. Insects, unlike birds and bats, cannot repair wing damage and therefore require compensatory control strategies from coupled neural and mechanical systems. For instance, dragonflies, moths, bees, and flies can readily compensate for a host of wing injuries in flight (3, 5, 7–10), but the underlying neural and mechanical strategies to compensate for wing damage remain elusive.

Insects, such as flies, are robust to naturally occurring wing damage, which can be achieved by tuned closed-loop control driven by sensory feedback. Robust control could enable flies to maintain performance without changes in internal neural gains (11). From an engineering perspective, flies might implement such a “robust control law,” which could maintain stability and appropriate performance for a certain range of wing damage without changes in internal control. Alternatively, they might adaptively change their internal gains over time to maintain adequate performance. Under such a scheme,

<sup>1</sup>Department of Mechanical Engineering, The Pennsylvania State University, University Park, PA 16802, USA. <sup>2</sup>Department of Mechanical Engineering, University of Colorado Boulder, Boulder, CO 80309, USA

\*Corresponding author. Email: jmmongeau@psu.edu

flies might implement an “adaptive control law,” similar to how airplanes change autopilot control parameters as mass decreases because of fuel consumption over the course of a flight (12). While these two hypotheses are not mutually exclusive, i.e., flies could use both strategies, teasing out their relative contribution is of great relevance to understanding the control principles of flapping flight. These principles could aid in the development of control schemes to enable flapping robots to compensate for damage.

Here, we applied a control theoretic framework to reveal how sensory feedback enables flies to compensate for wing damage in flight. To quantify how wing damage affects flight performance, we quantified the gaze stabilization response of flies with intact and unilaterally damaged wings. To facilitate input-output system analysis, we placed flies in a virtual reality magnetic tether, which permits rotation about the vertical axis and allows flies to close the loop between visual perturbations and body motion. Following unilateral wing area loss up to ~40%, flies exhibited only a modest decrease in flight performance during smooth movement and saccades. Flies compensated for unilateral wing damage by altering wingbeat amplitude (WBA), abdominal angle, and wingbeat frequency. By combining flight data in open- and closed-loop experimental paradigms with mathematical and robotic models, we show that asymmetric changes in WBA and bilaterally symmetric changes in wingbeat frequency are due to both active and passive mechanisms. Using control theory, we show that compensation to wing damage is achieved by an adaptive increase in damping that trades off performance and stability.

## RESULTS

### Unilateral wing damage marginally decreases gaze stabilization performance

To study the influence of wing damage on flight performance, we first sought to determine the tuning of the body’s yaw optomotor reflex in intact flies by presenting a broadband visual chirp stimulus to magnetically tethered flies (Fig. 1A). The frequency of the chirp stimulus logarithmically increased from 0.1 to 6.5 Hz over 20 s and was presented at a constant amplitude of 15°, representing peak speeds between 9° and 612° s<sup>-1</sup>, which are within the visual bandwidth limits of the yaw optomotor response of *Drosophila* (13, 14) (Fig. 1B).

Copyright © 2022  
The Authors, some  
rights reserved;  
exclusive licensee  
American Association  
for the Advancement  
of Science. No claim to  
original U.S. Government  
Works. Distributed  
under a Creative  
Commons Attribution  
NonCommercial  
License 4.0 (CC BY-NC).

Downloaded from https://www.science.org on November 20, 2024

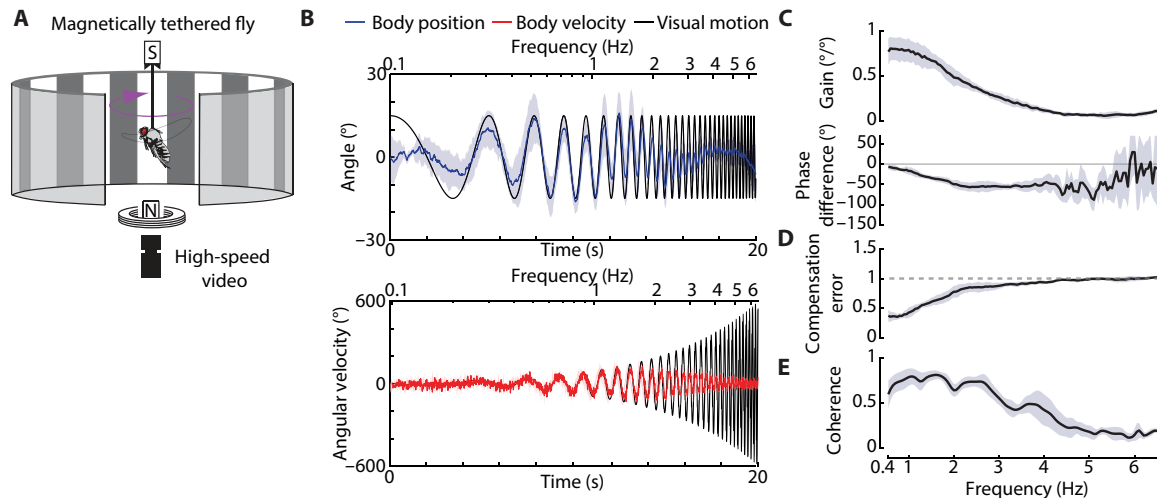


**Fig. 1. The yaw optomotor reflex is tuned to low frequencies.** (A) Magnetic tether system to study the optomotor response. Flies were glued to a magnetic pin and suspended between two magnets, thus enabling body motion about yaw (purple arrow). A virtual reality arena is used to play a visual stimulus to elicit an optomotor response. A high-speed camera was used to track changes in the fly heading. (B) Average fly angular position (blue) and velocity (red) to a visual chirp stimulus (black) for intact flies. The chirp started at a frequency of 0.1 Hz and increased logarithmically to 6.1 Hz. (C) Closed-loop gain and phase difference of the fly optomotor response. (D) Compensation error, defined as the vector distance in the complex plane from perfect compensation (gain = 1 and phase = 0°). Dashed line: Deleterious region indicates the compensation error (>1) where a fly's response degrades gaze stabilization more so than if the fly did nothing. (E) Coherence between the chirp stimulus and body motion. For (B) to (E), shaded region is  $\pm 1$  SD.  $n = 5$  flies.

For the chirp, we let velocity vary as the visuomotor response of *Drosophila* is velocity sensitive (13). This stimulus elicited an optomotor response at all frequencies, but the response was primarily tuned to low frequencies (peak speeds of  $38^\circ$  to  $188^\circ \text{ s}^{-1}$ ), representing the region with the highest gain and coherence, a measure of linear correlation in the frequency domain to evaluate linearity between input and output (see Materials and Methods), and the lowest compensation error, a performance metrics that combines gain and phase (see Materials and Methods; Fig. 1, C to E). At low frequencies, the closed-loop gain was close to unity and the phase difference was approximately zero, indicative of high compensation performance. However, as the stimulus frequency increased, both the gain and phase difference decreased rapidly, corresponding to a decrease in compensation performance. Above 4 Hz (peak angular velocity of  $377^\circ \text{ s}^{-1}$ ), the gain and coherence were near zero, and the phase difference became extremely noisy, suggesting that flies hardly respond to visual motion in this higher frequency band (Fig. 1, C to E). Below 0.4 Hz (peak angular velocity of  $28^\circ \text{ s}^{-1}$ ), flies responded to each step of individual pixels of the light-emitting diode (LED) arena; thus, the stimulus did not elicit smooth movement and had overall low coherence, further pointing to nonlinearities (Fig. 1C and fig. S1A). We therefore focused our further analyses to frequencies above this threshold. However, unlike canonical linear time-invariant systems, gaze control in flies is sensitive to visual motion amplitude, speed, and frequency (15, 16); thus, we sought to study the yaw optomotor response within a stimulus space that avoided saturation nonlinearities (either motor or sensory in origin). For a fly operating about a putative equilibrium point (e.g., zero retinal image velocity), such nonlinearities would not be naturalistic, as they would be pushing the fly near its performance limits (either motor or sensory) (17).

We next studied how unilateral wing damage could influence the performance of the optomotor response. To provide higher

signal-to-noise ratio than chirp stimuli, we generated a pseudo-random sum-of-sines stimulus. This stimulus was composed of nine logarithmically spaced and superimposed sine signals with random phase at each frequency (frequency range: 0.35 to 13.7 Hz; fig. S1B). To avoid exceeding the cutoff frequency (and speed) of the body of the fly and thereby saturation nonlinearities, the amplitude at each frequency was normalized by a mean angular velocity of  $52^\circ \text{ s}^{-1}$ , which resulted in a peak velocity of  $380^\circ \text{ s}^{-1}$  (fig. S1B). These experiments were conducted on two separate groups of flies with intact and unilaterally damaged wings (chordwise cut of the left wing; range: 10 to 40% area loss; Fig. 2A and movies S1 and S2).

We observed that damaged flies drifted slowly in the direction of the damaged wing (left; Fig. 2, B and C, and movie S2). In contrast, intact flies exhibited smaller drift, which occurred in an arbitrary direction, approximately equally in the clockwise and counterclockwise directions (Fig. 2C and movie S1). As the optomotor response is guided by a velocity-based controller that minimizes velocity or "slip" of the moving background onto the eye (18), the net velocity of the continuous drift can be interpreted as a flight performance deficit due to wing damage.

To tease apart the observed drift and flight performance following wing damage, we analyzed the angular velocity of both groups. Both groups demonstrated similar performance across a range of frequencies of the stimulus. However, the closed-loop gain substantially dropped at 3.7 Hz for both groups of flies, indicative of low-pass filtering (Fig. 2D). The phase difference gradually increased in the same manner for both groups with increasing frequency, again resembling a low-pass filter. A statistical comparison of the performance of intact and damaged flies yielded a significant difference in gain across all frequencies but not in phase difference (Fig. 2D and table S1). Furthermore, damaged flies compensation error was similar to intact flies (Fig. 2D and table S1). These results point to a modest decrease in gaze stabilization performance following unilateral wing damage.

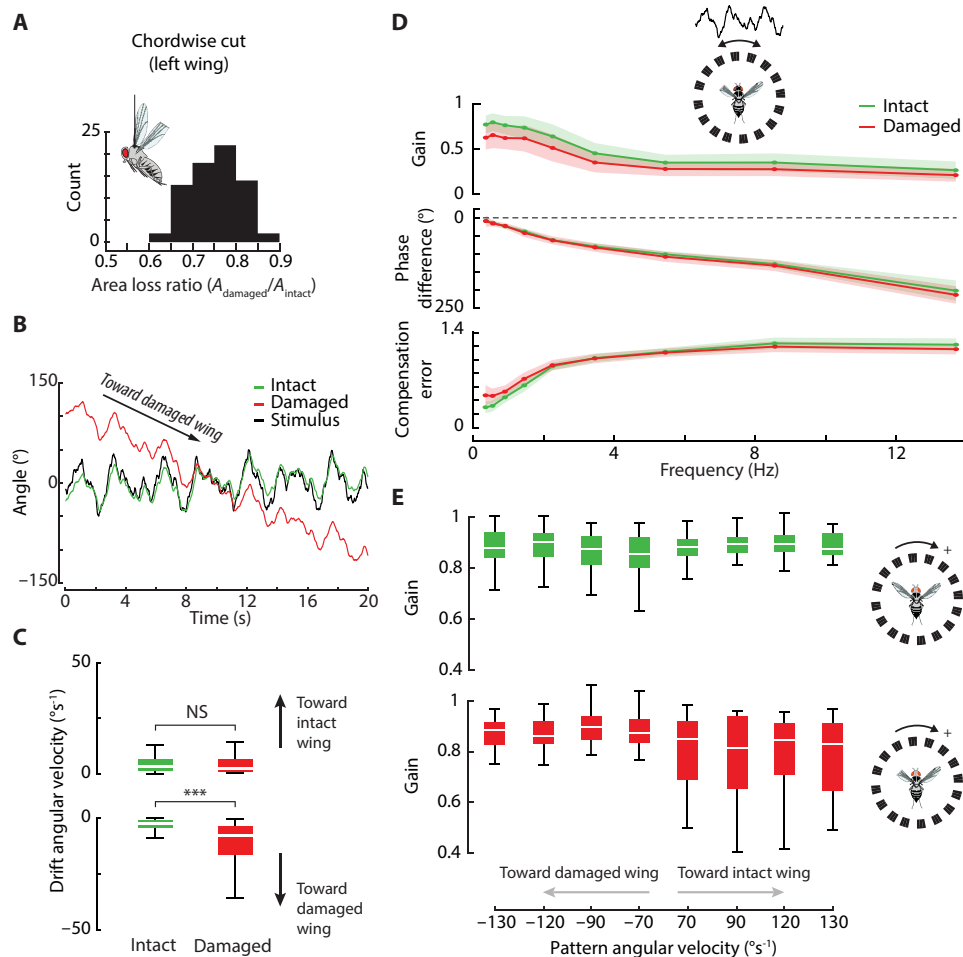


**Fig. 2. Unilateral wing damage modestly decreases stabilization performance.** (A) Histogram of the degree of unilateral wing damage ( $n = 71$  flies). (B) Average response for intact and damaged flies to a sum-of-sines visual stimulus (black). Damaged flies drifted toward the damaged (left) wing. (C) Box plot of the drift for both intact (green) and damaged (red) flies grouped by direction. Intact flies drifted in both direction (clockwise and counterclockwise) nearly equally (194 and 136 trials, respectively), whereas damaged flies drifted mostly toward the damaged wing (toward intact wing: 47 trials; toward damaged wing: 221 trials). Damaged flies exhibited a significantly larger drift toward the damaged wing. (D) Closed-loop gain, phase difference, and compensation error for intact (green) and damaged (red) flies in response to a sum-of-sines stimulus. Shaded error region is  $\pm 1$  SD. Wing damage had a significant influence on body gain but not on phase difference (see table S1 for statistics). (E) Gain of intact (top) and damaged (bottom) flies for smooth movement gaze stabilization experiments. Gain: Fly velocity/panorama velocity. Motion in the positive direction (toward the intact wing) generated significantly higher variance in gains in damaged flies compared to the intact group ( $F$  test,  $P < 0.001$  for all speeds). For (A) to (C), intact,  $n = 40$  (green) and damaged,  $n = 38$  (red). For (D), intact,  $n = 40$  and damaged,  $n = 38$ . For (E), intact,  $n = 25$  and damaged,  $n = 22$ . NS, not significant.

To measure how the degree of wing damage altered flight performance, we categorized flies with similar amounts of wing damage. Flies were placed into one of three groups (fig. S2A): flies with more than 30% of their wing area removed, flies with 30 to 20% of wing area removed, and flies with less than 20% of their wing area removed, corresponding to wing area ratios of  $<0.7$ ,  $0.7$  to  $0.8$ , and  $>0.8$ , respectively. Here, area ratio is defined as the ratio of the damaged wing area to the intact wing area. A statistical analysis revealed no significant difference between the gains and phase difference of the three groups for all frequencies (table S2). These results suggest that flies that lost around 40% of their total wing area performed similarly to flies that had lost only 10%.

To further investigate the impact of wing damage on tethered flight performance, we measured the number of stable and unstable flies in the magnetic tether for intact and damaged conditions. We

categorically defined an unstable fly as one that would spin or shoo continuously and thus failed to stabilize a static background when placed in the magnetic tether. Human error in pin placement can cause flies to be unstable, which is most likely a result of the pin being offset from the longitudinal axis. From 78 flies with a damaged wing, 36 flies were unstable (46%). For 50 intact flies, 20 were unstable (40%). Statistical analysis revealed that these two proportions were not statistically significant ( $z$  test;  $P = 0.50$ ), thus providing some assurance that flies can readily compensate for damage even in tethered condition and that the proportion of stable flies was not biased between intact and damaged conditions. The average wing loss area ratio for the stable and unstable flies were not statistically different ( $t$  test,  $P = 0.14$ ). These results suggest that the amount of wing area lost had little impact on flight performance in the magnetic tether for flies that lost 40% or less area of a single wing (fig. S2, B and C).

While we found an overall decrease in performance in body rotation gain following unilateral wing damage, flies could compensate for the decrease in body rotation gain by adjusting head movements. Head movements in *Drosophila* have smaller visuomotor delays than wing movements and can reduce retinal slip by up to ~60%; thus, the head could readily compensate for asymmetries in wing torque production (15). By tracking the head orientation of magnetically tethered fruit flies with respect to a fixed vertical axis, we measured the head motion of both intact and damaged flies. A frequency domain analysis revealed that head motion of damaged flies did not increase to account for the reduction in body motion, and in particular, damaged flies had smaller gains particularly at higher frequencies (fig. S2D and table S3).

To determine whether the decrease in task performance generalized to other classes of stimuli, we measured the body response of flies to a panorama moving at constant velocity. Corroborating previous work, intact flies compensated for a moving background by nearly matching its velocity, yielding gains close to unity, where gain here is defined as the ratio of the fly velocity to background velocity (Fig. 2E) (14, 19). Curiously, in intact flies, the variance for counterclockwise rotation was higher than for clockwise rotation ( $F$  test,  $P < 0.001$ ). The gain and variance of damaged flies were dependent on the stimulus direction. Specifically, when flies rotated toward the intact wing, whereby the damaged wing acted as the “motor,” gains were not statistically significant from intact flies when applying a Bonferroni correction for multiple comparisons (Fig. 2E). We found no significant effect of stimulus direction on gains for all velocities, suggesting that flies compensate strongly for wing damage. However, motion in the positive direction (toward the intact wing) generated significantly higher variance in gains in damaged flies compared to the intact group ( $F$  test,  $P < 0.001$  for all speeds). This variability is likely due to the drift observed in damaged flies (Fig. 2, B and C). As in a previous study, we found that wing damage had only a very minor influence on saccade dynamics (fig. S6). Together, unilateral wing damage marginally decreased gaze stabilization performance.

### Sensory feedback and passive mechanics modulate WBA and wingbeat frequency following wing damage

Unilateral wing damage marginally decreases gaze stabilization performance, and flies might actively compensate for asymmetric torque production by modifying their wing kinematics. In free flight, *Drosophila hydei*, a larger species of fruit fly than *Drosophila melanogaster*, alter wing kinematics following unilateral wing damage (9). *D. hydei* increase wingbeat frequency and adjust wing motion asymmetrically to counteract roll torque imbalances due to a unilateral loss in aerodynamic surface. However, the extent by which these compensation strategies are driven by active or passive mechanisms remains unclear. For instance, an asymmetry between the stroke angles of the left and right wings might arise from differential drag forces due to a unilateral loss in wing aerodynamic surface. Furthermore, a decrease in wing inertia might be accompanied by a concomitant increase in wingbeat frequency due to an increase in the resonant frequency of the wing-thorax mechanical system (20) and therefore may not require active neural control. Seminal work showed that the frequency of oscillation of asynchronous muscle is near resonance without any neural feedback (21). We sought to resolve the potential influence of passive aerodynamic and mechanical effects on compensatory flight strategies. To achieve this, we compared the WBA [two-dimensional (2D) projection of stroke angle] and

wingbeat frequency of flies in a rigid and magnetic tether system. As these two paradigms provide different control topologies (open versus closed loop), comparison of flight behavior between these paradigms can provide unique insights into the contribution of sensory feedback in flight control (Fig. 3A) (17). We reasoned that if relative changes in WBA between intact and damaged flies were the same in the presence (magnetic tether) and deficit (rigid tether) of visual reafference and body mechanosensory feedback, then an increase in WBA would be best explained by passive mechanics, as opposed to active compensation. Similarly, if wingbeat frequency was the same in both paradigms, then passive mechanics might be the best explanation for changes in wingbeat frequency.

To tease out the contribution of active and passive mechanisms, we first compared WBA in the rigid and magnetic tether when flies were presented with a static visual pattern, thereby simulating hovering conditions. We quantified the change in WBA ( $\Delta$ WBA) between the left and the right wing. In both the rigid and magnetic tether, unilateral wing damage significantly increased the  $\Delta$ WBA between intact and damaged flies ( $t$  test,  $P = 0.01$  and  $P < 0.001$  for the rigid and magnetic tether, respectively) (Fig. 3B). However,  $\Delta$ WBA in the magnetic tether was significantly larger than in the rigid tether ( $t$  test,  $P < 0.001$ ). Together, these results suggest that passive aerodynamics and visual feedback both contributed to the increase in  $\Delta$ WBA. To reveal how visual feedback modulates  $\Delta$ WBA, we quantified the left and right WBA individually in both the rigid and magnetic tether (Fig. 3, C and D). The damaged (left) WBA was different in damaged flies between paradigms, suggesting that WBA modulations of the damaged wing are driven by both passive and active mechanisms ( $t$  test,  $P < 0.001$ ). Similarly, the intact (right) WBA was marginally smaller for damaged flies in the magnetic tether, suggesting that flies actively modulate the intact wing ( $t$  test,  $P = 0.01$ ). There was a significant decrease in the intact wing WBA of damaged flies in the rigid tether, but because the visual stimuli were identical for rigid flies with and without damage, mechanics or feedback of non-visual origin may be responsible (Fig. 3C). Together, these results show that both passive mechanics and sensory feedback underlie wing control following unilateral damage.

In both paradigms, we confirmed that unilateral wing damage elevated wingbeat frequency (Fig. 3D) (9, 22, 23). Wingbeat frequency in the rigid tether was measured using a wingbeat analyzer, whereas a microphone measured wingbeat frequency in the magnetic tether (see Materials and Methods). We confirmed that the microphone provided a robust estimate of wingbeat frequency by comparing the signal to our wingbeat analyzer as a benchmark (fig. S3). Following unilateral wing damage, the wingbeat frequency was no different between magnetically and rigidly tethered flies ( $t$  test,  $P = 0.45$ ; Fig. 3E). This result suggests that the increase in wingbeat frequency following wing damage may be a manifestation of a passive change in wing-thorax resonance.

In rigidly tethered flies, wingbeat frequency scaled with the amount of damage (linear regression,  $P = 0.01$ ; Fig. 3E). By ablating a portion of the wing, we effectively reduced the inertia of an oscillatory system composed of the two wings and the thorax. Previous work showed that wingbeat frequency scales with wing inertia, as predicted by a linear spring-mass-damper model (23). Consistent with this previous work, we modeled the wing-thorax system as a second order pendulum system with inertia and damping (see the Supplementary Materials). From this simplified model, we estimated that the natural frequency  $\omega_n$  should scale according to

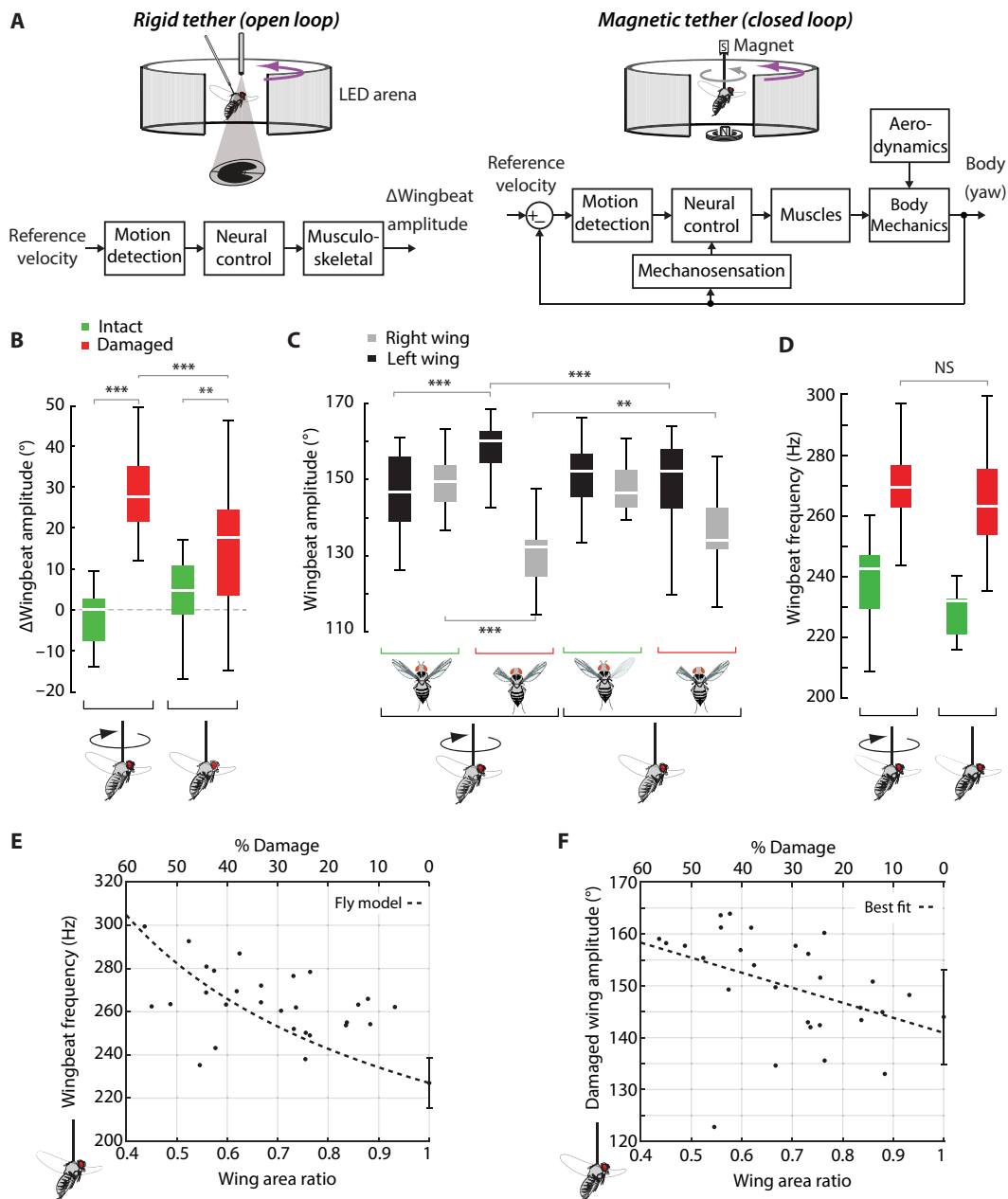


**Fig. 3. Sensory feedback and passive mechanics modulate wingbeat amplitude and frequency to compensate for wing damage.** (A) Top: Open- (rigid tether) and closed-loop (magnetic tether) experimental paradigms to study contribution of passive and active compensation. Bottom: Proposed control diagrams for each paradigm, adapted from (55). The closed-loop paradigm enables body rotation, which can be sensed by mechanosensors, e.g., halteres. (B) Wingbeat amplitude in the rigid (left) and magnetic (right) tether for intact (green) and damaged (red) flies. Rigid tether: Intact,  $n = 10$  and damaged,  $n = 28$ . Magnetic tether: Intact,  $n = 33$  and damaged,  $n = 30$ . (C) Wingbeat amplitude of individual wings for the magnetic (left) and rigid (right) tether. Green, intact; red, damaged; gray, right wing; black, left wing. Same data as (B). (D) Same as (B) but for wingbeat frequency. Rigid tether: Intact,  $n = 16$  and damaged,  $n = 30$ . Magnetic tether: Intact,  $n = 23$  and damaged,  $n = 33$ . (E) Relationship between wing damage and wingbeat frequency for rigidly tethered flies. For details on the fly model, see the Supplementary Materials. (F) Relationship between wing damage and wingbeat amplitude of rigidly tethered flies (for the left damaged wing).  $n = 28$  flies with damage and  $n = 10$  intact flies. For (E) and (F), error bars are shown for intact flies (wing area ratio = 1).

$$\omega_n = \frac{k}{l\sqrt{A_r}} \quad (1)$$

where  $k$  is a constant that accounts for the torsional stiffness of the wing joint,  $l$  is the wingspan, and  $A_r$  is the wing area ratio. Although this simplified mechanical model could explain some of the variance ( $R^2 = 0.22$ ), the high variance in wingbeat frequency is likely

because it is under active control and because flies need not flap at wing-thorax resonance. Rigidly tethered flies can actively modulate wingbeat frequency because of changes in visual and gyroscopic feedback (24, 25). Another possibility is that variation in flight kinematics reflects distinct flight control strategies of individual flies. Therefore, changes in wingbeat frequency following wing damage

are likely a manifestation of both passive and active mechanisms. Similarly, the wingbeat amplitude of the damaged (left) wing increased with the amount of damage, although there was considerable variability (linear regression,  $P = 0.022$ ;  $R^2 = 0.178$ ; Fig. 3F). By combining fly data with mathematical models, our data suggest that both active visual control and passive mechanics underlie flight strategies to compensate for wing damage.

### Wing kinematics are influenced by wing damage in an insect-inspired resonant system and aeromechanics model

Like flies, insect-scale flapping wing robots are subject to passive mechanical scaling because of wing damage. Previous work demonstrated the implications of nonlinear aerodynamic damping and its effect on flapping amplitude and frequency using spring-mass-damper lumped models (26–28). Furthermore, studies showed how changing wing aerodynamics and inertia together influence resonance for the design of micro air vehicles (26, 27). To reveal the extent to which passive mechanisms influence wing kinematics in an insect-inspired resonant mechanical system, we developed a robophysical model (fig. S4A). Both the robotic wing and the fruit fly wing operated in a similar dynamical regime in air [fly wing Reynolds number ( $Re$ ) =  $\sim 120$ ; robot wing  $Re = 500$  to  $600$  at resonance], and thus, the robot model can provide insights into the contribution of unsteady aerodynamics at the insect scale, despite having different wing kinematics and not being dynamically scaled to *D. melanogaster*. Furthermore, because the robot is open loop by design, it can provide a baseline for the contribution of passive mechanisms in shaping wing kinematics in a resonant system. Supporting the contribution of passive mechanics, the resonant wingbeat frequency of the robophysical model scaled with the amount of wing damage, as predicted by a linear aeromechanics model with quasi-steady assumptions (see the Supplementary Materials; fig. S4B). Corroborating previous work with a similar robot (29), the robophysical and aeromechanics model likewise exhibited an increase in wingbeat amplitude with an increase in wing damage (fig. S4C), although higher damage caused a saturation nonlinearity because of wing hinge geometry constraints (see the Supplementary Materials). Despite the simplified quasi-steady aeromechanical model, the close agreement between the model and physical prototype suggests that unsteady aerodynamics may play little role in shaping passive wing kinematics following a loss in aerodynamic surface. Together, the robophysical model provides insight into how wing kinematics are modulated passively in an insect-inspired resonant system.

### Wing damage causes a compensatory abdominal response of nonvisual origin

In addition, flies with damaged wings shifted the position of their abdomen by about  $9^\circ$  toward the intact wing, pointing to active compensation following wing damage (Fig. 4A). This compensatory strategy moved the center of mass toward the intact wing. In contrast, the abdomen of intact flies remained, on average, aligned to the long axis of the body. To determine whether the abdominal response might be driven by nonvisual senses, e.g., mechanosensory feedback from the damaged wing, we repeated the same experiment in the rigid tether system. As in the magnetic tether, the abdominal response of damaged and intact flies in the rigid tether was significantly different ( $t$  test,  $P < 0.001$ ; Fig. 4A). The abdominal response of damaged flies in the rigid tether scaled with wing damage, which itself scaled with  $\Delta WBA$  (Fig. 3), suggesting that wing damage drives

a compensatory abdominal response of nonvisual origin (Fig. 4B). Together, these results support the hypothesis that a shift in abdomen position is driven by a mechanosensory-based reflex loop between the wings and abdomen.

### Compensation strategy to wing damage suggests adaptive control

We showed that unilateral wing area loss as large as 40% leads to modest changes in overall flight performance during gaze stabilization (Fig. 2). In particular, we showed that active and passive mechanisms underlie changes in wing kinematics to balance aerodynamic forces generated by the damaged (left) and intact (right) wing (Fig. 3). From a control engineering standpoint, compensating for internal perturbations (e.g., change in aerodynamic surface of a wing) can be implemented via careful controller design. One strategy is to implement robust control to maintain function in the presence of known uncertainties (30). By carefully choosing controller parameters, one can demonstrate bounds within which a system will remain stable and maintain function without having to change controller parameters. Another strategy is to implement adaptive control, whereby function is maintained in the presence of unpredictable uncertainties. A hallmark of adaptive control systems is that the controller parameters are not fixed: They change in response to changes in system dynamics and uncertainties (12). Specifically, adaptive control allows for a system to change controller gains to achieve similar closed-loop performance, e.g., following changes to the body (plant) that could be due to damage.

To determine whether the neural controller of flies might be adaptive to our imposed perturbations, i.e., controller parameters change because of wing damage, we derived parametric frequency response functions (FRFs) of individual flies. Using the derived FRFs, we estimated the parameters of the internal neural controller and body dynamics (Fig. 5A). Specifically, by fitting a transfer function to the

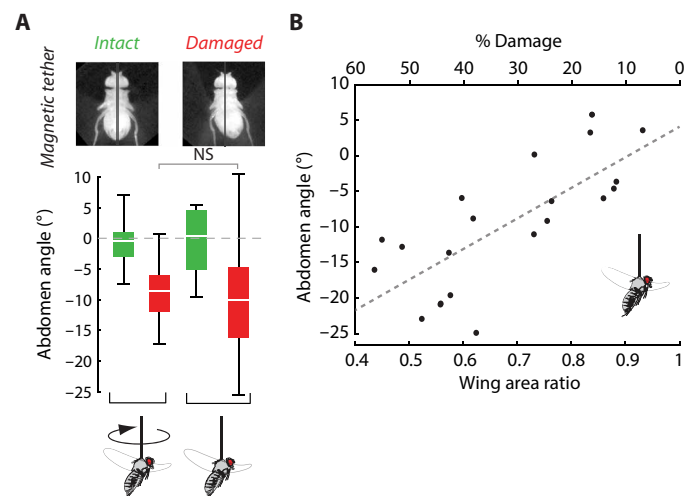


**Fig. 4. Wing damage causes a compensatory abdominal response of nonvisual origin.** (A) Top: Single frames from a trial in the magnetic tether. Bottom: Box plot of abdomen angle following wing damage in the rigid and magnetic tether. Magnetic tether: Intact,  $n = 40$  and damaged,  $n = 38$ . Rigid tether: Intact,  $n = 10$  and damaged,  $n = 21$ . (B) Scaling of abdomen angle with wing damage in the rigid tether. Dotted line is best-fit line ( $R^2 = 0.56$ ,  $P < 0.001$ ). Same rigid tether data as (A).

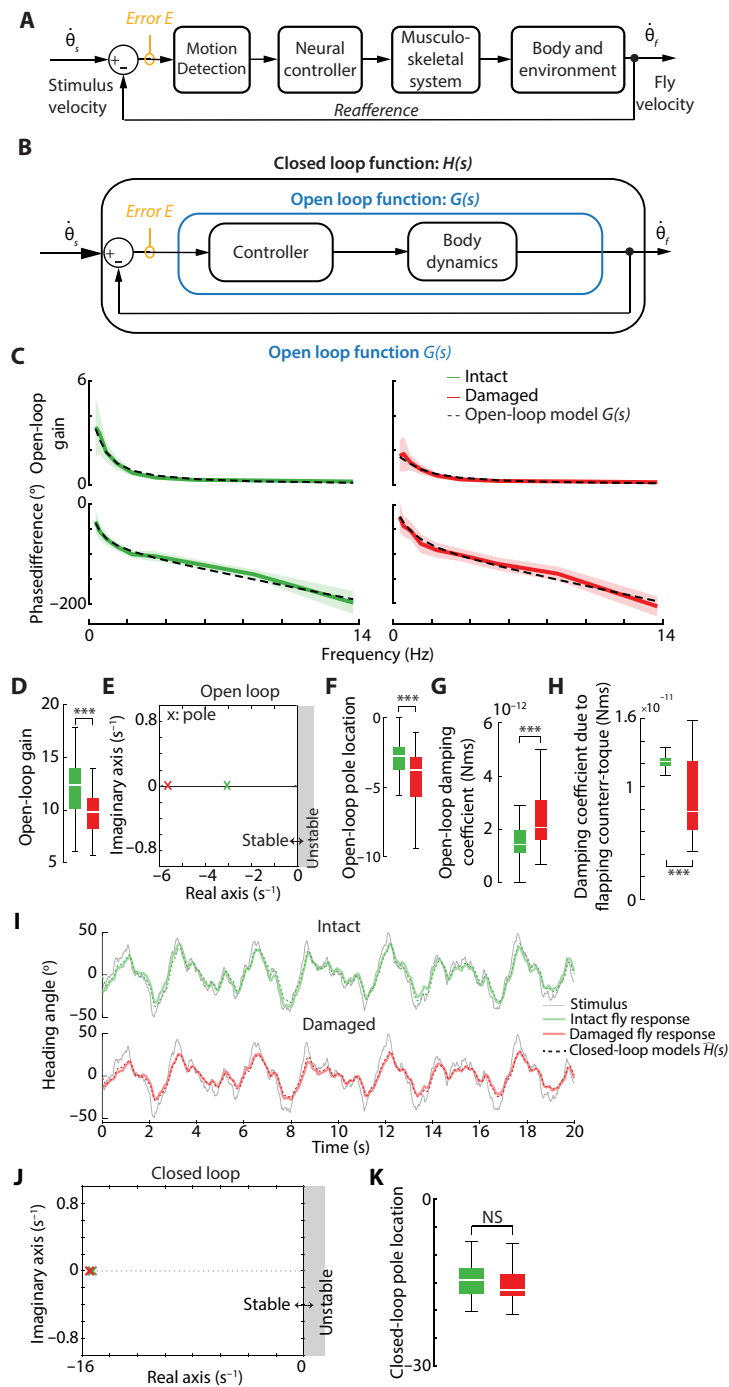


**Fig. 5. Compensation strategy trades off stability and performance.** (A) Proposed control diagram of the yaw optomotor reflex illustrating the input-output relationship of magnetically tethered flies. (B) The simplified system separated into two block diagrams, the neural controller, and body dynamics, which encompasses wing-thorax biomechanics and aerodynamics. The open-loop transfer function  $G(s)$  was estimated from the measured closed-loop transfer function  $H(s)$  using the frequency domain data generated from the sum-of-sines experiments. (C) The open-loop gain and phase of the open-loop transfer function for intact (left) and damaged flies (right). The open-loop transfer function was generated from experimental data shown in Fig. 2A (solid line). Green line, intact; red line, damaged; black dashed line, best-fit transfer function ( $R^2 = 0.90$  and  $0.89$  for intact and damaged flies, respectively). Shaded region is  $\pm 1$  SD. (D) Estimated open-loop gains for intact and damaged flies ( $t$  test,  $P < 0.001$ ). (E) Pole-zero map of the open-loop fit transfer functions. Both transfer functions are stable (poles in left-half plane) but with different coefficients. The poles are shown at the mean location across all flies. (F) Open-loop pole location for intact (green) and damaged (red) flies. (G) The open-loop damping coefficient of intact (green) and damaged flies (red). (H) Comparison of damping coefficients of intact and damaged estimated using a flapping counter-torque model. (I) Simulation of the closed-loop system estimated from the empirical open-loop transfer functions (Eqs. 3 and 4). Dashed line, simulation; solid lines, stimulus (gray) and actual fly responses (green, intact; red, damaged). (J) Pole-zero map of the closed-loop transfer function for intact (green) and damaged (red) flies. The pole is shown at the mean location across all flies. (K) Closed-loop pole location for intact (green) and damaged (red) flies. For all panels, intact,  $n = 40$  flies and damaged,  $n = 38$  flies.

empirical FRF, we estimated the open-loop transfer function  $G(s)$  of intact and damaged flies. The open-loop transfer function  $G$  is

$$G = \frac{\dot{\theta}_f}{E} \quad (2)$$

where  $\dot{\theta}_f$  is the angular velocity of the fly and  $E$  is the error or difference between the fly angular velocity and stimulus angular velocity  $\dot{\theta}_s$  (for clarity, the complex frequency  $s$  is omitted; Fig. 5A). We fit transfer functions of different orders to the frequency domain data and determined that the best fit was a first-order transfer function with no zeros, a single pole, and a time delay (see Materials and Methods), where the pole is the root of the denominator, which determines the stability of the system. Increasing the order of the transfer function did not significantly improve the fit accuracy. For instance, fitting the data to a transfer function with one zero and two poles (one of which is at the origin) allowed us to model the internal controller as a proportional-integral controller (fig. S5, A to C). The integral gain was significantly smaller than the proportional gain and, in some flies, was not different from zero (fig. S5C). This suggests that a first-order model with no zeroes can parsimoniously capture the dynamics of yaw gaze stabilization in fly flight. A first-order model is consistent with the notion that flies are sensitive to optic flow (velocity) and that the yaw optomotor response is dominated by aerodynamic damping (18). Thus, our proposed model is based on proportional (P) feedback control, where the fly's turning torque is proportional to the error  $E$ , with the system dynamics determined by the ratio of inertia and damping (see Eqs. 7 to 9 and the Supplementary Materials). The best-fit, open-loop transfer functions to the experimental data yielded

$$G_{\text{intact}} = \underbrace{e^{-0.021s}}_{\text{Delay}} \underbrace{\frac{12.2}{s + 3.1}}_{\text{Controller and body dynamics}} \quad (3)$$

and

$$G_{\text{damaged}} = e^{-0.22s} \frac{9.8}{s + 5.6} \quad (4)$$

where  $s$  is the complex frequency. While some individual animal variation was present, the variation was similar between intact and damaged flies (fig. S5D). Both models captured the overall dynamics of the behavioral data ( $R^2 \sim 90\%$ ; Fig. 5C).

By evaluating the numerator and denominator of  $G$ , we can acquire critical insights into how flies compensate for wing damage (see the Supplementary Materials). The numerator combines the neural controller gain and static gain of the body (plant), referred to as the open-loop gain. The denominator determines pole location and, thereby, the stability of intact and damaged flies. A statistical comparison of the intact and damaged open-loop gain yielded a significant decrease in gain in damaged flies (Fig. 5D and Table 1). A pole-zero map further revealed the different parameter (poles) between both open-loop systems despite both systems being stable (Fig. 5E). By pulling out the lowest denominator coefficients of both transfer functions, we estimated the damping coefficients of both groups of flies (see Materials and Methods). Damaged flies had an overall larger damping coefficient compared to intact flies (Fig. 5F), which could be due to an increase in wingbeat amplitude and frequency ( $t$  test,  $P < 0.001$ ) (9). To uncover the possible role of damping due to flapping following wing damage, we estimated the damping coefficient of intact and damaged flies based on a flapping-counter torque (FCT) model (see the Supplementary Materials) (31). In contrast to our experimental data, this model predicted an overall decrease in

**Table 1. Comparison of estimated parameters for intact and damaged flies.** Means  $\pm$  1 SD.

Controller parameter	Intact	Damaged	P value
Open-loop gain	12.21 $\pm$ 2.9	9.8 $\pm$ 2.3	1.3 $\times$ 10 <sup>-4</sup>
Damping coefficient (Nms)	1.6 $\pm$ 0.8 $\times$ 10 <sup>-12</sup>	2.9 $\pm$ 2.4 $\times$ 10 <sup>-12</sup>	5.8 $\times$ 10 <sup>-4</sup>

damping due to flapping motion following wing damage (Fig. 5G). Therefore, passive FCT effects themselves cannot explain the experimentally determined increase in damping. Together, these results indicate that wing damage not only alters the yaw gaze stabilization performance of flies but also modifies the coupled body dynamics and neural controller used to stabilize gaze.

At face value, it is not immediately clear why the open-loop gain decreases following wing damage, as both mechanics and neural control are coupled in flight. However, the open-loop system misses critical dynamics that are present in the closed-loop system. Flies operate in closed loop in the magnetic tether, and therefore, closed-loop stability and performance must be evaluated to contextualize the role of open-loop gains. To quantify how the changes in open-loop gain and damping influenced closed-loop performance, we substituted the empirical open-loop FRFs of intact and damaged flies (Eqs. 3 and 4) into the closed-loop system (Eq. 5). Specifically, we computed the closed-loop system response  $H$  from the empirically determined open-loop system  $G$  as

$$\hat{H} = \frac{G}{1+G} \quad (5)$$

(see the Supplementary Materials). Our simulation of the closed-loop systems  $\hat{H}$  demonstrated a very close match to the experimental data, further supporting our modeling choice and assumptions, e.g., linear time invariance (Fig. 5H). Evaluating  $\hat{H}_{\text{intact}}$  and  $\hat{H}_{\text{damaged}}$  yielded nearly identical pole locations for the two closed-loop systems (Fig. 5, I and J). This conclusion held when including a Padé approximation to the time delay (fig. S11). This analysis suggests that a decrease in gain in damaged flies has the benefit of maintaining stability at a level similar to intact flies. Therefore, flies trade off performance (decrease in closed-loop gain; Fig. 2D) and stability (similar pole location; Fig. 5J) by decreasing open-loop gain and actively increasing yaw damping.

## DISCUSSION

We found that flies compensate for extensive wing damage to one wing by modulating the neural control of damping, in a way analogous to human-engineered adaptive control systems. By combining mathematical modeling and experimental data, we show that damaged flies compensated for changes in wing aerodynamic surface by adjusting wingbeat amplitude and frequency, guided by both feedback control and passive mechanics (Fig. 3). Removing 10 to 40% of the area of a single wing modestly altered overall yaw gaze control performance during smooth movement (Fig. 3). Using a control theoretic framework, we demonstrate that damaged flies operate at a lower open-loop gain and, therefore, lower gaze compensation performance, but that this decrease in gain is accompanied by an active increase in damping that maintains stability at a level similar to intact flies (Fig. 5).

Our results suggest that flies can tolerate severe wing damage by modulating damping to maintain adequate stability and performance. By assuming a model of the body grounded in studies of yaw dynamics in *Drosophila*, our control theoretic approach enabled us to begin to describe the dynamically coupled neural controller and internal (body) dynamics. A decrease in open-loop gain decreased overall performance by producing smaller responses to the visual error (Fig. 5C). While a decrease in gain could be solely due to changes in body (plant) dynamics, when considering the closed-loop system, we show that the closed-loop pole locations are not statistically distinguishable between intact and damaged flies (Fig. 5, I and J). The similar location of poles concomitant with changes in damping support the hypothesis that damaged flies implement an adaptive control strategy via modulation of gains to maintain stability similar to intact flies. By modeling damping due to FCT, we predicted that damping should decrease following wing damage, but flies instead increased overall damping (Fig. 5, F and G). Notably, if passive mechanics were to dominate, then we would have expected flies with different amounts of wing damage to have different closed-loop pole locations because wingbeat frequency, which directly influences aerodynamic damping (32), increases with wing damage (Fig. 4B). These results suggest that active mechanism(s), other than FCT, increased damping. An interesting possibility is that damping is increased by haltere-based, inner-loop feedback (33), although body movement frequency may be below the threshold of the haltere system (13). In addition, the change in visuomotor gain described here is consistent with the notion that flies can adjust visuomotor gains to learn novel feedback dynamics, as demonstrated in seminal work using virtual reality closed-loop paradigms (34, 35). Overall, flies' coupled mechanics and neural compensation exhibit attributes analogous to robust and adaptive systems.

Our results support the notion that both passive mechanics and sensory feedback modulate wingbeat frequency and amplitude in response to wing damage. Following wing damage, we showed that wingbeat frequency was similar between magnetically and rigidly tethered flies (Fig. 3E), which suggests that the increase in wingbeat frequency is a manifestation of a passive change in wing-thorax resonance. This conclusion corroborates previous studies, which showed that wingbeat frequency scales with wing damage, as predicted by a linear mass-spring-damper model (9, 22, 23). Seminal work by Machin and Pringle (21) showed that this frequency modulation may be a property of asynchronous muscles because of delayed stretch activation. Recent work in tethered soldier flies showed that unilateral wing damage decreases wingbeat amplitude but does not change frequency but that bilateral wing damage increases wingbeat frequency (36, 37). Deora *et al.* (37) argued that the increase in wingbeat frequency following unilateral wing damage in freely flying *Drosophila* (9) could have been an active response due to loss of lift. However, our results suggests that this is not the case in *Drosophila* because tethered flies with unilateral wing damage experience a considerable increase in wingbeat frequency (Fig. 3E). Thus, fruit flies and soldier flies may rely on different wing regulation and coordination mechanisms.

We found that a loss in wing area corresponded to a scaled abdominal response of nonvisual origin. This result supports the hypothesis that a shift in abdomen position is driven by a mechanosensory-based reflex loop between the wings and abdomen. It is likely that the relative shift in sensor population that follows from loss of wing area elicits the abdominal response. The shift in abdomen position observed

in flies may be analogous to the wing-driven abdominal response in moths (38). At present, it is unclear how this reflex participates in yaw torque production, if at all, as its function could be obscured by the constraints of the magnetic tether. A previous study in free flight support the notion that *Drosophila* could generate small corrective yaw torques with their abdomen (39). Furthermore, hawk moths can use their abdomen for pitch stability (40). One possibility is that shifting the center of mass toward the intact wing helps modulate compensatory roll responses observed in free flight (9).

In the magnetic tether, flies generate yaw turning torque in response to visual motion, and at present, it is unclear whether the wing kinematics that produce turning are similar in free flight. Freely flying flies generate ballistic banked turns (saccades) primarily by adjusting the timing and magnitude of wing rotation angle (41, 42). To our knowledge, it is not known whether flies use a similar strategy to generate nonsaccadic smooth turns, as elicited in our experiments (Fig. 1). How flies modulate wing kinematics in the magnetic tether may be different from those in free flight because flies can only rotate about the yaw axis and cannot translate. However, under constant speed yaw visual rotation, visuomotor gains in the magnetic tether are similar to free flight gains (14, 19), suggesting that flies can compensate despite these constraints. The visuomotor gains in the magnetic tether are likely dependent on the steering capacity and, therefore, the wing motor capacity of the flies. In free flight, flies must regulate their altitude with changes in wing motion; however, previous studies have shown that maintaining rotational stability and executing fast rotational maneuvers require very little (or even negligible) increase in muscle energy output (43) and tiny changes in wing motion (41, 42). Therefore, we do not expect that maintaining altitude would affect the fly's steering capacity considerably. Because flies in the magnetic tether are not challenged by the need to support body weight or regulate other degrees of freedom such as roll, pitch, or side slip, our results must be interpreted with appropriate caution. An interesting avenue for future research will be to determine how flies in the magnetic tether control their wings, which may provide insights into the flexibility of flapping flight control in flies.

The notion that compensation to wing damage is a manifestation of adaptive changes in gain has important implications for the design of fault-tolerant insect-scale robots (44). For instance, it could inspire the design of closed-loop control algorithms for flapping robots with on-board vision. As in flies, flapping robots could be designed with active control of wing parameters and abdominal (e.g., tail) angle guided by stabilizing passive mechanics to rapidly compensate for wing damage (9, 45, 46) or with passive control such as passive aerodynamic drag balancing (47). Together, the fly-inspired strategies described here might enable the next generation of adaptive insect-scale robots to fly in uncertain environments.

## MATERIALS AND METHODS

### Animal preparation

Animal preparation was similar to previous work (19). In short, female fruit flies (*D. melanogaster*) aged 3 to 5 days were cold-anesthetized at 4°C and glued to a stainless-steel pin at the thorax. Flies rested for approximately 1 hour before the start of the experiments. After the rest period, flies were then suspended between two magnets inside a virtual reality arena (Fig. 1A) (48). The magnetic tether enabled flies to pivot about the yaw axis, while restricting motion in other directions. The inertia of the ferromagnetic pin is less than 1% of

the fly's inertia about the yaw axis (rod diameter = 100  $\mu\text{m}$  and tip diameter = 12.5  $\mu\text{m}$ ; Minutien pin, Fine Science Tools). The sapphire bearing provides a coefficient of friction of approximately  $\sim 0.1$  (Vee Jewel Bearing, Bird Precision), which flies can readily overcome (19). To investigate the effects of wing damage, we ablated a portion of the left wing along the width (chord-wise ablation) using 8-mm micro-scissors (Fine Science Tools). Only flies that successfully completed at least three trials were used in the analysis. Flies that were unstable because of excessive shaking, had a low WBA (lower than  $100^\circ$ ), or continuously stopped flapping their wings were not used in the analysis. After the experiments, damaged flies were cold-anesthetized again and had both wings removed at the base. The wings were placed flat under a microscope and imaged using a camera mounted on the microscope. A custom-written MATLAB routine was used to calculate the area of the intact and damaged wings. Overall, the amount of wing area removed was similar to previous work in free flight (9). Rigid tether preparations were conducted in a similar manner to previous studies (15). In short, female fruit flies with intact and damaged wings were glued to a tungsten pin. The wings were unilaterally damaged by clipping a small portion of the left wing along its width (chord-wise cut). Overall, flies with more than  $\sim 40\%$  wing area removed were unstable in the magnetic tether; hence, wing damage was restricted so that flies lost at most  $\sim 40\%$ .

### Stimuli and experimental setups: Magnetic tether

The virtual reality arena (48) allowed us to elicit an optomotor response by presenting flies with a moving visual stimulus (moving background). The background consisted of uniformly spaced bars with a spatial wavelength of  $22.5^\circ$  subtending onto the fly eye. To test the impact of wing damage, distinct stimuli were used to elicit an optomotor response. A chirp stimulus was initially used to gauge the frequency tuning of the optomotor response. The frequency of the chirp stimulus logarithmically increased for 0.1 to 6.1 Hz while maintaining a constant amplitude of  $15^\circ$ . On the basis of the results of the chirp analysis (Fig. 1), a second experiment was designed to test the impact of wing damage on flight performance at specific frequencies with higher signal-to-noise ratio (Fig. 1). We therefore designed a second experiment using a sum-of-sines stimulus. The stimulus was generated by summing nine single sine waves with frequencies that ranged from 0.35 to 13.7 Hz. The components of this stimulus had a random phase and an amplitude normalized by  $52^\circ \text{s}^{-1}$  to avoid saturating the visual and motor system. Each trial lasted 20 s and was presented eight times to each fly. Flies that could not complete at least three trials were not used in the analysis. A third set of experiments was conducted to measure flight performance when compensating for a background moving at constant velocity. The background was moved at five velocities from  $70^\circ$  to  $130^\circ \text{s}^{-1}$  in both the clockwise and counterclockwise directions. The heading of the fly was recorded using a bottom-view camera (Basler acA640-750  $\mu\text{m}$ ) at 80 to 160 frames  $\text{s}^{-1}$  (fps). Wing data were collected by measuring the wingbeat amplitude (extreme position at downstroke-to-upstroke reversal) using a modified version of Kinefly (16, 49). Wingbeat frequency was measured using a microphone (Polsen OLM-10) interfaced to an amplifier (Polsen PMA-1). The microphone was placed  $\sim 1$  cm directly above the fly. The output signal from the amplifier was recorded and digitally filtered with a high-pass filter with a cut-off frequency of 120 Hz. A fast Fourier transform (FFT) was used to estimate the flapping frequency from the filtered signal.

### Rigid tether

Rigidly tethered flies with intact and unilaterally damaged wings were placed inside a virtual reality arena. We presented flies with a static pattern composed of uniformly spaced bars with a spatial wavelength of  $22.5^\circ$ . A camera recording at 100 fps captured the wing blur motion, which enabled us to measure the wingbeat amplitude of each wing (WBA). The camera was placed below the fly so that measurements of wing angles were a 2D projection of stroke angles. In addition, a custom wingbeat analyzer recorded the wingbeat frequency by tracking the shadow of the left and right wings projected onto a photodiode. The wingbeat analyzer has been described previously in detail (50). Flies were exposed to a static background for 10 s, and each presentation was repeated three times.

### Tracking in the magnetic tether

The head and body motion of flies in the global reference frame were tracked using a custom-written MATLAB code (15). The left and right WBAs in both magnetically and rigidly tethered flies were tracked using custom software adapted from Kinefly (49, 51). WBA for each fly was determined by calculating the angle between the edge of the wing blur and the axis along the fly's body. Videos of magnetically tethered flies were first registered to eliminate yaw motion.

### Flight performance metrics

To quantify the impact of wing damage on flight performance, we calculated multiple performance metrics used in system identification of engineering systems (gain, phase difference, coherence, and compensation error). This analysis was conducted in MATLAB using custom-written code. The gain and phase difference were estimated using the FFT function. The gain was calculated by dividing the magnitude of the FFT of the output (heading of the fly) by the input (motion of the visual pattern). The phase difference was estimated by subtracting the phase of the output from that of the input. Coherence, a linear estimate of how much power is transferred from the input to the output of a system, was calculated using the built-in MATLAB function *mscohere*. Coherence was used as a metric to define the stimulus parameters, which avoided saturation nonlinearities. Last, we computed compensation error, a metric that combines both gain and phase (52). For a dynamic system, a gain of 1 and a phase difference of 0 indicate perfect tracking. Compensation error  $\epsilon$  is the vector distance in the complex plane (norm) between actual tracking performance  $H$  and perfect tracking  $Z_0$  expressed as

$$\epsilon = \|H - Z_0\| \quad (6)$$

Therefore, a compensation error of 0 indicates perfect tracking, whereas larger values indicate imperfect tracking. The gain, phase difference, coherence, and tracking error were estimated for each individual fly and then averaged out across all flies to determine the grand mean for every experimental condition.

### System and parameter identification

Because the magnetic tether restricts body motion to rotation about the yaw axis, this allowed us to approximate the body dynamics of the fly as a first-order differential equation

$$I\dot{\omega}(t) = -C\omega(t) + \tau(t) \quad (7)$$

where  $\omega$  is the angular velocity of the fly in yaw,  $\tau$  is the torque generated by the wings,  $I$  is the inertia of the fly about the yaw axis [ $5.2 \times 10^{-13}$  Nms<sup>2</sup>; (53)], and  $C$  is the damping coefficient about the yaw axis (or about the point of rotation offset from the center of mass in the magnetic tether). This model explicitly defines velocity as the state variable, which is consistent with the notion that the yaw optomotor reflex is sensitive to optic flow.

All transfer function fitting was performed using MATLAB (MathWorks Inc.). We fit the fly response to approximate the open-loop transfer function (Fig. 5, A and B) (54). The feedback error was calculated by subtracting the actual motion of the fly from the visual stimulus. This allowed us to approximate the internal, open-loop transfer function. A transfer function was fit to the empirical FRF using a modified least-square estimate in MATLAB. We tested transfer functions of different order but found that a first-order transfer function with a nonzero delay produced the best fit. The time delay accounts for the delay of the optomotor response and was set as a free parameter with a maximum of 0.8 s. Only fits with at least 65% goodness of fit ( $R^2$ ) were used in estimating controller parameters. The average  $R^2$  for intact flies was  $93 \pm 4.5$  and  $89 \pm 7.4\%$  for damaged flies (normalized root mean square error = 0.07 and 0.11, respectively). The frequency response of both intact and damaged flies was fit to a transfer function  $G(s)$  of the form

$$G(s) = \frac{b_0}{s + a_0} e^{-\tau_d s} \quad (8)$$

where  $a_0$  and  $b_0$  represent free parameters,  $e^{-\tau_d s}$  is the delay term with delay  $\tau_d$ , and  $s$  is the complex frequency. For a first-order mechanical system, we can estimate the damping coefficient through the following equality

$$a_0 = \frac{C}{I} \quad (9)$$

where  $C$  is the damping coefficient, and  $I$  is the yaw moment of inertia.

## Statistics

For all box plots, the central line is the median, the bottom and top edges of the box are the 25th and 75th percentiles, and the whiskers extend to  $\pm 2.7$  SDs. Unless otherwise specified, we report means  $\pm 1$  SD. Significant differences are stated as  $*P \leq 0.05$ ,  $**P \leq 0.01$ , and  $***P \leq 0.001$ .

**Note Added in Proof:** Recent work suggests that head movements in *Drosophila* are damped by the halteres [B. Cellini and J.-M. Mongeau, Nested mechanosensory feedback actively damps visually guided head movements in *Drosophila*. *Elife* **11**, (2022); <https://doi.org/10.7554/eLife.80880>].

## SUPPLEMENTARY MATERIALS

Supplementary material for this article is available at <https://science.org/doi/10.1126/sciadv.abo0719>

[View/request a protocol for this paper from Bio-protocol.](#)

## REFERENCES AND NOTES

- R. V. Cartar, Morphological senescence and longevity: An experiment relating wing wear and life span in foraging wild bumble bees. *J. Anim. Ecol.* **61**, 225 (1992).
- P. A. Fleming, D. Muller, P. W. Bateman, Leave it all behind: A taxonomic perspective of autotomy in invertebrates. *Biol. Rev. Camb. Philos. Soc.* **82**, 481–510 (2007).
- S. A. Combes, J. D. Crall, S. Mukherjee, Dynamics of animal movement in an ecological context: Dragonfly wing damage reduces flight performance and predation success. *Biol. Lett.* **6**, 426–429 (2010).
- H. Rajabi, J.-H. Dirks, S. N. Gorb, Insect wing damage: Causes, consequences and compensatory mechanisms. *J. Exp. Biol.* **223**, jeb215194 (2020).
- A. M. Mountcastle, T. M. Alexander, C. M. Switzer, S. A. Combes, Wing wear reduces bumblebee flight performance in a dynamic obstacle course. *Biol. Lett.* **12**, (2016).
- H.-N. Wehmann, T. Engels, F.-O. Lehmann, Flight activity and age cause wing damage in house flies. *J. Exp. Biol.*, (2021).
- M. J. Fernandez, D. Springthorpe, T. L. Hedrick, Neuromuscular and biomechanical compensation for wing asymmetry in insect hovering flight. *J. Exp. Biol.* **215**, 3631–3638 (2012).
- K. Kihlström, B. Aiello, E. Warrant, S. Sponberg, A. Stöckl, Wing damage affects flight kinematics but not flower tracking performance in hummingbird hawkmoths. *J. Exp. Biol.* **224**, jeb236240 (2021).
- F. T. Muijres, N. A. Iwasaki, M. J. Elzinga, J. M. Melis, M. H. Dickinson, Flies compensate for unilateral wing damage through modular adjustments of wing and body kinematics. *Interface Focus* **7**, 20160103 (2017).
- M.-B. Leonte, A. Leonhardt, A. Borst, A. S. Mauss, Aerial course stabilization is impaired in motion-blind flies. *J. Exp. Biol.* **224**, jeb242219 (2021).
- I. Uyanik, S. Sefati, S. A. Stamper, K.-A. Cho, M. M. Ankarali, E. S. Fortune, N. J. Cowan, Variability in locomotor dynamics reveals the critical role of feedback in task control. *eLife* **9**, e51219 (2020).
- K. J. Åström, B. Wittenmark, *Adaptive Control* (Dover Publications, ed. 2, 2008).
- A. Sherman, M. H. Dickinson, A comparison of visual and haltere-mediated equilibrium reflexes in the fruit fly *Drosophila melanogaster*. *J. Exp. Biol.* **206**, 295–302 (2003).
- M. Mronz, F. O. Lehmann, The free-flight response of *Drosophila* to motion of the visual environment. *J. Exp. Biol.* **211**, 2026–2045 (2008).
- B. Cellini, J.-M. Mongeau, Active vision shapes and coordinates flight motor responses in flies. *Proc. Natl. Acad. Sci. U.S.A.* **117**, 23085–23095 (2020).
- B. Cellini, W. Salem, J.-M. Mongeau, Complementary feedback control enables effective gaze stabilization in animals. *Proc. Natl. Acad. Sci. U.S.A.* **119**, e2121660119 (2022).
- E. Roth, S. Sponberg, N. Cowan, A comparative approach to closed-loop computation. *Curr. Opin. Neurobiol.* **25**, 54–62 (2014).
- M. H. Dickinson, F. T. Muijres, The aerodynamics and control of free flight manoeuvres in *Drosophila*. *Philos. Trans. R. Soc. B Biol. Sci.* **371**, 20150388 (2016).
- J. M. Mongeau, M. A. Frye, *Drosophila* spatiotemporally integrates visual signals to control saccades. *Curr. Biol.* **27**, 2901–2914.e2 (2017).
- R. Dudley, *The Biomechanics of Insect Flight: Form, Function, Evolution* (Princeton University Press, 2002).
- K. E. Machin, J. W. S. Pringle, The physiology of insect fibrillar muscle—II Mechanical properties of a beetle flight muscle. *Proc. R. Soc. London. Ser. B. Biol. Sci.* **151**, 204–225 (1959).
- O. Sotavalta, Flight-tone and wing-stroke frequency of insects and the dynamics of insect flight. *Nature* **170**, 1057–1058 (1952).
- C. H. Greenewalt, The wings of insects and birds as mechanical oscillators. *Proc. Am. Philos. Soc.* **104**, 605–611 (1960).
- B. J. Duisterma, M. B. Reiser, Y. Zhu, M. A. Frye, Dynamic properties of large-field and small-field optomotor flight responses in *Drosophila*. *J. Comp. Physiol. A Neuroethol. Sens. Neural Behav. Physiol.* **193**, 787–799 (2007).
- J. Bartussek, A. K. Mutlu, M. Zapotocky, S. N. Fry, Limit-cycle-based control of the myogenic wingbeat rhythm in the fruit fly *Drosophila*. *J. R. Soc. Interface* **10**, 20121013 (2013).
- D. Campolo, M. Azhar, G.-K. Lau, M. Sitti, Can DC motors directly drive flapping wings at high frequency and large wing strokes? *IEEE/ASME Trans. Mechatronics* **19**, 109–120 (2014).
- J. Zhang, X. Deng, Resonance principle for the design of flapping wing micro air vehicles. *IEEE Trans. Robot.* **33**, 183–197 (2017).
- J. Lynch, J. Gau, S. Sponberg, N. Gravish, Dimensional analysis of spring-wing systems reveals performance metrics for resonant flapping-wing flight. *J. R. Soc. Interface* **18**, 20200888 (2021).
- S. Chopra, N. Gravish, Piezoelectric actuators with on-board sensing for micro-robotic applications. *Smart Mater. Struct.* **28**, 115036 (2019).
- K. J. Åström, R. M. Murray, *Feedback Systems: An Introduction for Scientists and Engineers* (Princeton University Press, 2010).
- T. L. Hedrick, B. Cheng, X. Deng, Wingbeat time and the scaling of passive rotational damping in flapping flight. *Science* **324**, 252–255 (2009).
- B. Cheng, S. N. Fry, Q. Huang, W. Dickson, M. Dickinson, X. Deng, Turning dynamics and passive damping in flapping flight. *Proc. IEEE Int. Conf. Robot. Autom.*, 1889–1896 (2009).
- M. J. Elzinga, W. B. Dickson, M. H. Dickinson, The influence of sensory delay on the yaw dynamics of a flapping insect. *J. R. Soc. Interface* **9**, 1685–1696 (2012).
- M. Heisenberg, R. Wolf, *Vision in Drosophila: Genetics of Microbehavior* (Springer, 1984).
- R. Wolf, A. Voss, S. Hein, M. Heisenberg, Can a fly ride a bicycle? *Philos. Trans. R. Soc. London. Ser. B Biol. Sci.* **337**, 261–269 (1992).

36. T. Deora, A. K. Singh, S. P. Sane, Biomechanical basis of wing and haltere coordination in flies. *Proc. Natl. Acad. Sci. U.S.A.* **112**, 1481–1486 (2015).
37. T. Deora, S. S. Sane, S. P. Sane, Wings and halteres act as coupled dual oscillators in flies. *eLife* **10**, e53824 (2021).
38. B. H. Dickerson, Z. N. Aldworth, T. L. Daniel, Control of moth flight posture is mediated by wing mechanosensory feedback. *J. Exp. Biol.* **217**, 2301–2308 (2014).
39. R. Berthé, F.-O. Lehmann, Body appendages fine-tune posture and moments in freely manoeuvring fruit flies. *J. Exp. Biol.* **218**, 3295–3307 (2015).
40. J. P. Dyhr, K. A. Morgansen, T. L. Daniel, N. J. Cowan, Flexible strategies for flight control: An active role for the abdomen. *J. Exp. Biol.* **216**, 1523–1536 (2013).
41. A. J. Bergou, L. Ristroph, J. Guckenheimer, I. Cohen, Z. J. Wang, Fruit flies modulate passive wing pitching to generate in-flight turns. *Phys. Rev. Lett.* **104**, 148101 (2010).
42. F. T. Muijres, M. J. Elzinga, N. A. Iwasaki, M. H. Dickinson, Body saccades of *Drosophila* consist of stereotyped banked turns. *J. Exp. Biol.* **218**, 864–875 (2015).
43. P. Liu, B. Cheng, Limitations of rotational manoeuvrability in insects and hummingbirds: evaluating the effects of neuro-biomechanical delays and muscle mechanical power. *J. R. Soc. Interface* **14**, 20170068 (2017).
44. K. Jayaram, J. Shum, S. Castellanos, E. F. Helbling, R. J. Wood, Scaling down an insect-size microrobot, HAMR-VI into HAMR-Jr. arXiv:2003.03337v1 [cs.RO] (6 Mar 2020).
45. P. Chirarattananon, K. Y. Ma, R. J. Wood, Adaptive control of a millimeter-scale flapping-wing robot. *Bioinspir. Biomim.* **9**, 025004 (2014).
46. P. Chirarattananon, K. Y. Ma, R. J. Wood, Perching with a robotic insect using adaptive tracking control and iterative learning control. *Int. J. Rob. Res.* **35**, 1185–1206 (2016).
47. P. S. Sreetharan, R. J. Wood, Passive aerodynamic drag balancing in a flapping-wing robotic insect. *J. Mech. Des.* **132**, 051006 (2010).
48. M. B. Reiser, M. H. Dickinson, A modular display system for insect behavioral neuroscience. *J. Neurosci. Methods* **167**, 127–139 (2008).
49. M. P. Suver, A. Huda, N. Iwasaki, S. Safarik, M. H. Dickinson, An array of descending visual interneurons encoding self-motion in *Drosophila*. *J. Neurosci.* **36**, 11768–11780 (2016).
50. M. H. Dickinson, F. O. Lehmann, K. G. Götz, The active control of wing rotation by *Drosophila*. *J. Exp. Biol.* **182**, 173–189 (1993).
51. B. Cellini, W. Salem, J.-M. Mongeau, Mechanisms of punctuated vision in fly flight. *Curr. Biol.* **31**, 4009–4024.e3 (2021).
52. E. Roth, K. Zhuang, S. A. Stamper, E. S. Fortune, N. J. Cowan, Stimulus predictability mediates a switch in locomotor smooth pursuit performance for *Eigenmannia virescens*. *J. Exp. Biol.* **214**, 1170–1180 (2011).
53. J. A. Bender, M. H. Dickinson, Visual stimulation of saccades in magnetically tethered *Drosophila*. *J. Exp. Biol.* **209**, 3170–3182 (2006).
54. E. Roth, M. B. Reiser, M. H. Dickinson, N. J. Cowan, in *2012 IEEE 51st IEEE Conference on Decision and Control (CDC)* (IEEE, 2012), pp. 3721–3726; <http://ieeexplore.ieee.org/document/6426231/>.
55. B. Cellini, J.-M. Mongeau, Hybrid visual control in fly flight: Insights into gaze shift via saccades. *Curr. Opin. Insect Sci.* **42**, 23–31 (2020).
56. N. T. Jafferis, E. F. Helbling, M. Karpelson, R. J. Wood, Untethered flight of an insect-sized flapping-wing microscale aerial vehicle. *Nature* **570**, 491–495 (2019).
57. N. Gravish, Y. Chen, S. A. Combes, R. J. Wood, *2014 IEEE/RSJ International Conference on Intelligent Robots and Systems* (IEEE, 2014), pp. 3397–3403; <http://ieeexplore.ieee.org/document/6943035/>.
58. K. Y. Ma, P. Chirarattananon, S. B. Fuller, R. J. Wood, Controlled flight of a biologically inspired, insect-scale robot. *Science* **340**, 603–607 (2013).
59. Y. Chen, K. Ma, R. J. Wood, in *2016 IEEE/RSJ International Conference on Intelligent Robots and Systems (IROS)* (IEEE, 2016), pp. 2329–2336; <http://ieeexplore.ieee.org/document/7759363/>.
60. Y. Chen, N. Gravish, A. L. Desbiens, R. Malka, R. J. Wood, Experimental and computational studies of the aerodynamic performance of a flapping and passively rotating insect wing. *J. Fluid Mech.* **791**, 1–33 (2016).
61. R. J. Wood, S. Avadhanula, R. Sahai, E. Steltz, R. S. Fearing, Microrobot design using fiber reinforced composites. *J. Mech. Des.* **130**, 052304 (2008).
62. J. P. Whitney, P. S. Sreetharan, K. Y. Ma, R. J. Wood, Pop-up book MEMS. *J. Microeng. Microfab.* **21**, 115021 (2011).
63. A. Mathis, P. Mamidanna, K. M. Cury, T. Abe, V. N. Murthy, M. W. Mathis, M. Bethge, DeepLabCut: Markerless pose estimation of user-defined body parts with deep learning. *Nat. Neurosci.* **21**, 1281–1289 (2018).
64. A. L. Desbiens, Yufeng Chen, R. J. Wood, in *2013 IEEE/RSJ International Conference on Intelligent Robots and Systems* (IEEE, 2013), pp. 1367–1373; <http://ieeexplore.ieee.org/document/6696527/>.
65. D. Ishihara, T. Horie, M. Denda, A two-dimensional computational study on the fluid–structure interaction cause of wing pitch changes in dipteran flapping flight. *J. Exp. Biol.* **212**, 1–10 (2009).
66. K. Sum Wu, J. Nowak, K. S. Breuer, Scaling of the performance of insect-inspired passive-pitching flapping wings. *J. R. Soc. Interface* **16**, 20190609 (2019).
67. T. S. Collett, M. F. Land, Visual control of flight behaviour in the hoverfly *Syrirta pipiens* L. *J. Comp. Physiol. A* **99**, 1–66 (1975).
68. J. A. Bender, M. H. Dickinson, A comparison of visual and haltere-mediated feedback in the control of body saccades in *Drosophila melanogaster*. *J. Exp. Biol.* **209**, 4597–4606 (2006).
69. L. V. Hedges, Distribution theory for glass's estimator of effect size and related estimators. *J. Educ. Stat.* **6**, 107–128 (1981).
70. B. M. Finio, N. O. Perez-Arancibia, R. J. Wood, in *2011 IEEE/RSJ International Conference on Intelligent Robots and Systems* (IEEE, 2011), pp. 1107–1114; <http://ieeexplore.ieee.org/document/6094421/>.
71. J. P. Whitney, R. J. Wood, Aeromechanics of passive rotation in flapping flight. *J. Fluid Mech.* **660**, 197–220 (2010).
72. M. H. Dickinson, F.-O. Lehmann, S. P. Sane, Wing rotation and the aerodynamic basis of insect flight. *Science* **284**, 1954–1960 (1999).

**Acknowledgments:** We thank V. Le and S. Xu for laboratory assistance. We also thank N. Cowan for comments on a previous draft of the manuscript. **Funding:** This material is based on work supported by the Air Force Office of Scientific Research under award number FA9550-20-1-0084 and Alfred P. Sloan Research Fellowship (FG-2021-16388) to J.-M.M. **Author contributions:** Conceptualization: W.S. and J.-M.M. Data collection: W.S., B.Ce., and H.K. Data analysis: W.S., B.Ce., H.K.H.P., and J.-M.M. Writing: W.S., B.Ch, K.J., and J.-M.M. **Competing interests:** The authors declare that they have no competing interests. **Data and materials availability:** All data needed to evaluate the conclusions in the paper are present in the paper and/or the Supplementary Materials. All data, code, and materials used in the analyses are available through Penn State Scholar Sphere (DOI: 10.26207/exer-0k60).

Submitted 12 January 2022  
Accepted 30 September 2022  
Published 18 November 2022  
10.1126/sciadv.abo0719